# Half-Life Systematics across the $N = 126$ Shell Closure: Role of First-Forbidden Transitions in the $\beta$ Decay of Heavy Neutron-Rich Nuclei

A. I. Morales,[1,*] J. Benlliure,[1] T. Kurtukián-Nieto,[1,†] K.-H Schmidt,[2] S. Verma,[1,‡] P. H. Regan,[3,4] Z. Podolyák,[3] M. Górska,[2] S. Pietri,[3,§] R. Kumar,[5,2] E. Casarejos,[1,¶] N. Al-Dahan,[3] A. Algora,[6,7] N. Alkhomashi,[3,**] H. Álvarez-Pol,[1] G. Benzoni,[8] A. Blazhev,[9] P. Boutachkov,[2] A. M. Bruce,[10] L. S. Cáceres,[2] I. J. Cullen,[3] A. M. Denis Bacelar,[10] P. Doornenbal,[2] M. E. Estévez-Aguado,[1] G. Farrelly,[3] Y. Fujita,[11] A. B. Garnsworthy,[3] W. Gelletly,[3] J. Gerl,[2] J. Grebosz,[12] R. Hoischen,[13] I. Kojouharov,[2] N. Kurz,[2] S. Lalkovski,[10] Z. Liu,[14] C. Mihai,[15] F. Molina,[6,††] D. Mücher,[9,‡‡] B. Rubio,[6] H. Shaffner,[2] S. J. Steer,[3] A. Tamii,[16] S. Tashenov,[2] J. J. Valiente-Dobón,[17] P. M. Walker,[3] H. J. Wollersheim,[2] and P. J. Woods[14]

[1]*Universidade de Santiago de Compostela, E-15782 Santiago de Compostela, Spain*
[2]*GSI, Planckstrasse 1, D-64291 Darmstadt, Germany*
[3]*Department of Physics, University of Surrey, Guildford GU2 7XH, United Kingdom*
[4]*National Physical Laboratory, Teddington, Middlesex TW11 0LW, United Kingdom*
[5]*IFAC, New Delhi, India*
[6]*IFIC, CSIC-Universidad de Valencia, E-46071 Valencia, Spain*
[7]*Institute of Nuclear Research of the Hungarian Academy of Sciences, Debrecen H-4001, Hungary*
[8]*INFN, Università degli Studi di Milano, I-20133 Milano, Italy*
[9]*IKP, University of Cologne, D-50937 Cologne, Germany*
[10]*School of Computing, Engineering and Mathematics, University of Brighton, Brighton BN2 4GJ, United Kingdom*
[11]*Department of Physics, Osaka University, 560-0043 Osaka, Japan*
[12]*The Henryk Niewodniczànski Institute of Nuclear Physics, PL-31-342 Kraków, Poland*
[13]*Department of Physics, Lund University, S-22100 Lund, Sweden*
[14]*School of Physics and Astronomy, University of Edinburgh, Edinburgh EH9 3JZ, United Kingdom*
[15]*Horia Hulubei National Institute of Physics and Nuclear Engineering (IFIN-HH), RO-077125 Bucharest-Magurele, Romania*
[16]*Research Center for Nuclear Physics (RCNP), Osaka University, 567-0047 Osaka, Japan*
[17]*INFN-Laboratori Nazionali di Legnaro, I-35020 Legnaro, Italy*

(Received 25 February 2014; published 11 July 2014)

This Letter reports on a systematic study of $\beta$-decay half-lives of neutron-rich nuclei around doubly magic $^{208}$Pb. The lifetimes of the 126-neutron shell isotone $^{204}$Pt and the neighboring $^{200–202}$Ir, $^{203}$Pt, $^{204}$Au are presented together with other 19 half-lives measured during the "stopped beam" campaign of the rare isotope investigations at GSI collaboration. The results constrain the main nuclear theories used in calculations of $r$-process nucleosynthesis. Predictions based on a statistical macroscopic description of the first-forbidden $\beta$ strength reveal significant deviations for most of the nuclei with $N < 126$. In contrast, theories including a fully microscopic treatment of allowed and first-forbidden transitions reproduce more satisfactorily the trend in the measured half-lives for the nuclei in this region, where the $r$-process pathway passes through during $\beta$ decay back to stability.

DOI: 10.1103/PhysRevLett.113.022702 PACS numbers: 25.70.Mn, 23.40.-s, 26.30.Hj, 27.80.+w

In very hot, neutron-rich stellar environments, the $r$ process of nucleosynthesis is ignited in a series of rapid neutron captures on seed nuclei of the Fe group, thus creating very exotic neutron-rich nuclei that $\beta$ decay back to stability around the neutron shell closures with $N = 50$, 82, and 126. In these "waiting-point" regions, matter is accumulated at masses $A \sim 80$, 130, and 195, thus creating the so-called first, second, and third $r$-abundance peaks. These basic features of the $r$ process were established more than half a century ago [1]. However, how the heavy nuclei from Ni to U are synthesized is one of the major unanswered questions of modern physics because of the large uncertainties in the path, time scale, and astrophysical conditions for the rapid neutron capture process to develop [2]. Observational constraints such as the elemental abundances in metal-poor stars or in solar system material help to determine astronomical sites where it might occur [3,4]. Concurrently, $\beta$-decay properties of very exotic nuclei near the path, such as $\beta$ half-lives, are critical in determining the observed abundances [5]. Since many of the $r$-process progenitors cannot be accessed with present radioactive ion beam facilities, estimates of $r$-process nucleosynthesis generally rely upon predictions of state-of-the-art nuclear models, based on the properties of nuclei far from stability [6–11]. But at extreme values of isospin, theoretical predictions may be biased by microscopic structural effects that modify the shape of the $\beta$-strength function, such as nuclear shell quenching or deformation [12,13]. Until now, such theories have only been tested with information on $\beta$ decay around the first two waiting points

 

at $N = 50$ and 82 [13–20]. However, no results are available for the $\beta$ decays near the $A \sim 195$ $r$-abundance peak. New information on the $\beta$ decay of moderately neutron-rich $N \sim 126$ nuclei is, thus, very important to help model the underlying nuclear structure in this stretch of the $r$-process pathway and, also, to determine the relative abundances of nuclei in the third $r$-process peak [5].

The $\beta$-decay model most often used for nucleosynthesis calculations is the FRDM + QRPA model [6]. It is based on the microscopic quasiparticle random-phase approximation and the macroscopic finite-range droplet mass model to account for the Gamow-Teller part of the $\beta$-strength function. First-forbidden contributions are incorporated only macroscopically, using the statistical gross theory as a perturbation of the main Gamow-Teller strength. Calculated half-lives exceed the measured values for nuclei near the $A \sim 80$ and 130 waiting points by a factor of 2 or more, suggesting that the description of the first-forbidden strength is not optimal [18–20]. Larger discrepancies are expected for the $A \sim 195$ $r$-process nuclei [7], where first-forbidden transitions may significantly influence the low-energy spectra due to the opening of the intruder $\pi 0i_{13/2}$ state near the Fermi surface. Hence, particular attention is paid to models that incorporate allowed and first-forbidden transitions in the same microscopic framework. These are the DF3 + cQRPA model [7,8] that implements the continuum QRPA (cQRPA) on top of the Fayans energy density functional (DF3), the spherical QRPA with realistic forces for the proton-neutron interaction ($pn$-QRPA) [11], and the shell model (SM) [21], employed to calculate half-lives for semimagic, $N = 126$ nuclei with a variety of truncations of the model space [9,10]. Although all these approaches find the contribution of first-forbidden decays crucial in reducing the predicted lifetimes, the discrepancies for the $N = 126$ $r$-process waiting-point nuclei are still greater than those in the $N = 50$ and 82 regions [11].

From an experimental viewpoint, half-lives represent the first accessible property for nuclei at the current limits of experimental synthesis. The use of cold fragmentation reactions [22,23] combined with analysis techniques developed *ad hoc* for in-flight experiments [24] has enabled, after many years, the measurement of half-lives in the neutron-rich region around $^{208}$Pb. In the present Letter, we report on the half-lives of $^{200–202}$Ir, $^{203,204}$Pt, and $^{204}$Au, four of which, $^{200,201}$Ir and $^{203,204}$Pt, have been measured for the first time. The nucleus $^{204}$Pt is the lightest $N = 126$ isotone for which $\beta$-decay data are presently available. These results are combined together with other 19 half-lives measured during the "stopped beam" campaign of the rare isotope investigations at GSI (RISING) collaboration [25–30] to provide the first systematic comparison with theoretical predictions across the $N = 126$ shell closure. The location of the nuclei in the Segrè chart is shown in Fig. 1.

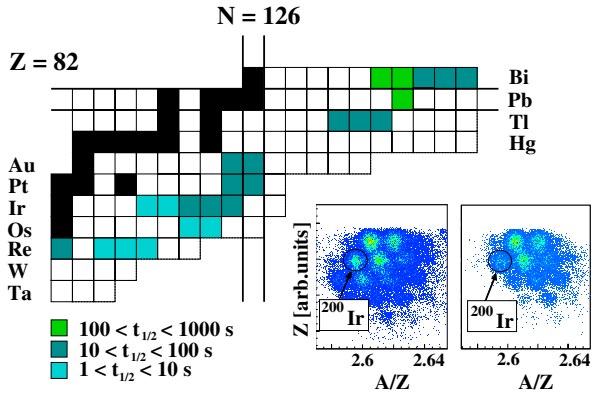


FIG. 1 (color online). Neutron-rich $N \sim 126$ region analyzed during the stopped beam RISING campaign. Measured half-lives are shown in color scale. Inset: Identification plots for $Z$ as a function of $A/Z$ at the final focal plane of the separator (left) and in the active stopper (right).

Neutron-rich $N \sim 126$ nuclei were produced at the Gesellschaft für Schwerionenforschung (GSI, Darmstadt), following cold fragmentation reactions of a 1 A · GeV $^{208}$Pb primary beam from the SIS-18 synchrotron with a 2.5 g/cm$^2$ Be target. The beam intensity was typically $10^8$ s$^{-1}$, delivered in cycles of 10 s with spills of 2 s. The residues were identified in flight in the fragment separator [31], specifically tuned to transmit $^{202}$Ir along its central trajectory. At the exit of the spectrometer a decay station, consisting of an active stopper detection system [32] enclosed by the RISING $\gamma$-ray array in its stopped beam configuration [33], was set up. The energy, time, and position of all the nuclear species implanted in the active stopper were recorded on an event-by-event basis. This information was also collected for $\beta$ particles and coincident $\gamma$ rays in order to define correlations in position and time for the extraction of $\beta$-decay half-lives. Details of the equipment, identification, and correlation procedures can be found in previous publications [27,29,34,35]. Here, we show the identification matrices at the exit of the separator and in the active stopper (Fig. 1, inset panel).

In relativistic in-flight fragmentation experiments, $\beta$ half-lives must be orders of magnitude smaller than the implantation rates for the delayed-coincidence technique to be efficiently applied. While in lighter-mass regions this condition is fulfilled, for $N \sim 126$ nuclei lifetimes can significantly exceed the beam cycles. Accordingly, a large amount of $\beta$ activity builds up, and the extraction of half-lives with conventional analytical fits, e.g., with exponential-time distribution functions, is no longer valid. Alternative procedures for data analysis, developed specially for experiments with complex background conditions, must then be employed.

The so-called numerical method developed by T. Kurtukián-Nieto *et al.* [24] has been used to determine half-lives for the present data set. This technique evaluates

complex time-correlated structures using Monte Carlo simulations of experimental ion-$\beta(\gamma)$ correlations. These correspond to the time elapsed between implantations and subsequent $\gamma$ transitions in the $\beta$-decay daughter. Two types of time spectra are sorted for the experimental and simulated data, the first including normal ion-$\beta(\gamma)$ time differences and the second including correlations between implantations and preceding $\gamma$ transitions in the daughter nucleus, henceforth called $\beta(\gamma)$-ion correlations. Since the two distributions are influenced by the half-life of the nucleus in different ways, their ratio is a unique fingerprint carrying information on the $\beta$-decay half-life of interest. This ratio is, therefore, used in the fits: Several numerical ratios determined from the simulation and corresponding to different values of the lifetime are compared to the experimental ratio. Lifetimes are then calculated from a $\chi^2$ minimization. Further details on the performance, limits of application, and testing of the method have been reported elsewhere [24,27].

Time-correlated spectra for the $N = 126$ isotone $^{204}$Pt and the neighboring $^{202}$Ir and $^{200}$Ir nuclei are presented in the left part of Fig. 2. The solid line indicates ion-$\beta(\gamma)$ time distributions, whereas the dashed line shows $\beta(\gamma)$-ion time correlations. The ion-$\beta(\gamma)$ distribution of $^{202}$Ir is fitted to a double-exponential function corresponding to the $\beta$-decay curve plus an exponential background. The half-life of this nucleus is 1 order-of-magnitude smaller than the implantation rates, and hence, there is no activity buildup arising from multiple-fragment random correlations in the $\beta$-decay curve. Similarly to the $^{218}$Bi case [27], the decay of $^{202}$Ir is used to cross-check the numerical technique with standard analytical procedures. The agreement between both results, $t_{1/2}^{\mathrm{an}} = 16.0(17)$ s and $t_{1/2}^{\mathrm{num}} = 15(3)$ s, benchmarks the capabilities of the numerical method. The numerical fit is illustrated in the right-hand side of Fig. 2. Experimental ratios are shown in dots, whereas the numerical fitting function is displayed as a continuous line. The $\chi^2$ minimizations, shown in the inset panels, provide half-lives of $t_{1/2} = 16^{+6}_{-5}$ s for $^{204}$Pt and $t_{1/2} = 43(6)$ s for $^{200}$Ir. It should be noted, as well, that the current measurements of $^{202}$Ir, $t_{1/2} = 15(3)$ s, and $^{204}$Au, $t_{1/2} = 37.2(8)$ s, agree with the previous reported values of $t_{1/2} = 11(3)$ s [25] and $t_{1/2} = 39.8(9)$ s [36] within 2 standard deviations, thus providing an additional verification of the method.

The results of the present work are shown in Table I together with a compilation of half-lives measured with the stopped beam RISING setup [25–30]. Half-lives for $^{194-196}$Re, $^{199,200}$Os, $^{199-202}$Ir, $^{203,204}$Pt, $^{211-213}$Tl, and $^{219}$Bi were determined either for the first time or with improved accuracy during the experimental campaign. These half-lives are compared to the predictions of the theoretical

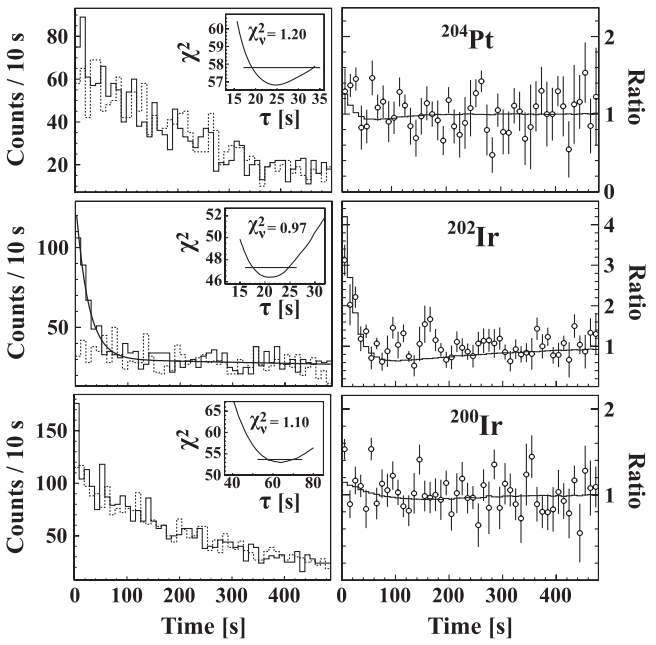


FIG. 2. Left part: Measured ion-$\beta(\gamma)$ (solid line) and $\beta(\gamma)$-ion (dashed line) time correlations. The exponential fit to the ion-$\beta(\gamma)$ time-correlated spectrum of $^{202}$Ir is shown in the figure. Right part: Experimental ratios between ion-$\beta(\gamma)$ and $\beta(\gamma)$-ion time distributions (dots) and simulated numerical ratios minimizing the $\chi^2$ test (continuous line). The $\chi^2$ minimizations are shown in the insets. The straight lines denote the uncertainty of the measured half-lives. The reduced $\chi^2$ values are also provided.

TABLE I. Comparison of measured $N \sim 126$ half-lives [25–30] with predicted values of FRDM + QRPA($a$) [6], DF3 + cQRPA ($b$) [7,8], $pn$-QRPA ($c$) [11], and SM ($d$) [9,37].

| Nucleus | $t_{1/2}^{\mathrm{exp}}$ (s) | $t_{1/2}^{(a)}$ (s) | $t_{1/2}^{(b)}$ (s) | $t_{1/2}^{(c)}$ (s) | $t_{1/2}^{(d)}$ (s) |
|---|---|---|---|---|---|
| $^{192}$Re | 16(2) | 54 | 7.7 | ... | ... |
| $^{194}$Re | 6(1) | 71 | 2.1 | ... | ... |
| $^{195}$Re | 6(1) | 3.2 | 8.5 | 4.5 | ... |
| $^{196}$Re | $3^{+1}_{-2}$ | 3.6 | 1.4 | ... | ... |
| $^{199}$Os | $5^{+4}_{-2}$ | 107 | 6.6 | 30 | ... |
| $^{200}$Os | $6^{+4}_{-3}$ | 187 | 6.9 | 24 | ... |
| $^{198}$Ir | 8(3) | 377 | 19.1 | ... | ... |
| $^{199}$Ir | $6^{+5}_{-4}$ | 371 | 46.7 | 9.5 | ... |
| $^{200}$Ir | 43(6) | 124 | 25 | ... | ... |
| $^{201}$Ir | 21(5) | 130 | 28.4 | 3.9 | ... |
| $^{202}$Ir | 15(3) | 68 | 9.8 | ... | ... |
| $^{203}$Pt | 22(4) | 564 | 30.3 | 134 | 21.1 |
| $^{204}$Pt | $16^{+6}_{-5}$ | 322 | 16.4 | 81 | 16.4 |
| $^{204}$Au | 37.2(8) | 455 | 95 | ... | ... |
| $^{205}$Au | 32.5(14) | 222 | 29.8 | 7.5 | ... |
| $^{211}$Tl | $88^{+46}_{-29}$ | 71 | 115 | 33.7 | ... |
| $^{212}$Tl | $96^{+42}_{-38}$ | 29 | 13 | ... | ... |
| $^{213}$Tl | $46^{+55}_{-26}$ | 32 | 70 | 22.4 | ... |
| $^{215}$Pb | 160(40) | 283 | 165 | 225.3 | ... |
| $^{215}$Bi | 456(12) | 1102 | 295 | 660.7 | ... |
| $^{216}$Bi | 133(15) | 99 | 48 | ... | ... |
| $^{217}$Bi | 93(11) | 178 | 87 | 138.6 | ... |
| $^{218}$Bi | 33(6) | 3 | 19 | ... | ... |
| $^{219}$Bi | 22(7) | 27 | 14.7 | 38.9 | ... |

models cited in the introduction [6–9,11]. For DF3+cQRPA, the calculations include the energy-density functional and effective $NN$ interaction reported in Ref. [7], without any additional energy-dependent spreading width of the elementary excitations in the case of the Os-Au isotopes [8]. For $pn$-QRPA and SM, the renormalization and quenching factors are chosen according to the experimental data available in the $N = 82$ and 126 regions. An enhancement factor $\epsilon = 2.0$ for the rank-0 matrix element of $\gamma_5$ is also introduced in Refs. [9,11]. This value has been updated to $\epsilon = 1.5$ for the SM half-lives in Table I, which reproduces the present results better for $^{203,204}$Pt [37].

The systematic trends of measured and calculated half-lives are illustrated in Fig. 3. The FRDM + QRPA predictions, very often used in astrophysical $r$-process modeling, significantly overestimate the measured values for most of the $N < 126$ nuclei, while the predictions seem to be close to the experimental trend in the $N > 126$ region. This behavior can be understood in terms of the microscopic distribution of the $\beta$-decay strength function: In the $Z < 82$, $N < 126$ quadrant, $\beta$ transitions are mainly driven by the first-forbidden neutron-proton configurations $(\nu 2p_{1/2}, \pi 2s_{1/2})$, $(\nu 1f_{5/2}, \pi 1d_{3/2})$, and $(\nu 0i_{13/2}, \pi 0h_{11/2})$. They dominate the low-energy spectra of $N < 126$ nuclei because they are much more energetic than the main $(\nu 0h_{9/2}, \pi 0h_{11/2})$ Gamow-Teller component, which is additionally suppressed by the low transition energy and the large filling of the $0h_{11/2}$ proton orbital. This effect is still significant near the $N \sim 126$ $r$-process pathway. There, theoretical models estimate that the first-forbidden contribution can greatly exceed the 10% of the total decay

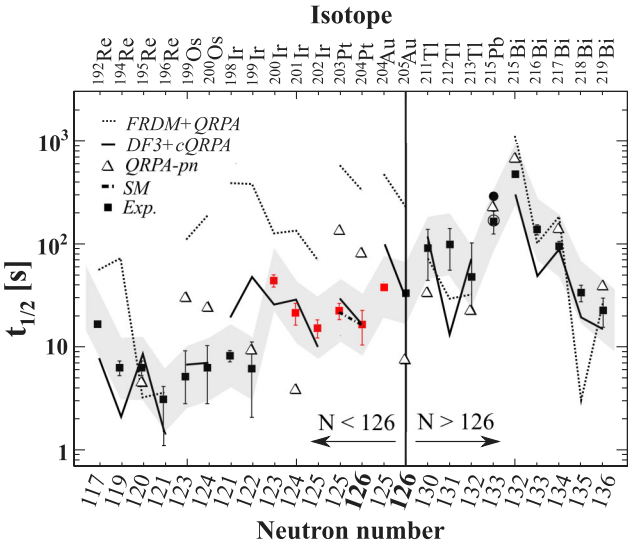


FIG. 3 (color online). Half-life systematics across the $N \sim 126$ shell closure. Results reported in this Letter are shown with red squares. For $^{215}$Pb, the FRDM and DF3 predictions are shown with filled and empty circles, respectively. Deviations up to a factor of 2 from the experimental values are indicated with a shaded area. See text for discussion.

width [6,7,9–11]. The situation is extreme for the $Z = 77$–79, $N \sim 126$ nuclei with moderate $Q_\beta$ values. In these cases, the main allowed contribution to the $\beta$-decay strength function lies outside the $Q_\beta$ window, and the total half-life is mainly determined by the first-forbidden part of the $\beta$ strength.

In a recent publication based on the same data [35], a partial $\beta$-decay scheme for $^{204}$Au was proposed from $\beta$-delayed $\gamma$ spectroscopy of the $N = 126$ isotone $^{204}$Pt. Shell model calculations for this $\beta$ decay indicate that all the levels are most likely fed through high-energy first-forbidden $\beta$ transitions, while the first states populated in allowed Gamow-Teller decays are spread out far above the $Q_\beta$ window. This is in agreement with the half-life presented in this Letter. The value calculated with the standard FRDM + QRPA model, which only includes Gamow-Teller $\beta$ transitions microscopically, exceeds the experimental result by more than 1 order of magnitude. Similarly, the half-lives of the Os-Au isotopes are overestimated by factors ranging from 3 to 60. This excess is independent of the odd-even behavior arising from the omission of the isosinglet nucleon-nucleon interaction in the model [8]. Instead, the minor role given to the first-forbidden $\beta$ strength can be seen as responsible for the large deviations: Systematic studies of partial $\beta$-decay schemes for some of these nuclei [35,36,38] indicate that the most intense $\beta$ transitions populate low-lying states of opposite parity, while weaker Gamow-Teller decays, if predicted to exist, feed levels at higher energies. For the Tl isotopes shown in Fig. 3, $\beta$ transitions to daughter states built on an $s_{1/2}$ proton excitation are completely blocked by the large spin difference, and the main contribution to the total $\beta$ strength is expected to be driven by the allowed single-particle $(\nu i_{11/2}, \pi i_{13/2})$ $\beta$ decay [29]. Again, the predictions of the FRDM + QRPA model deviate for the $Z \geq 82$ Pb and Bi isotopes. Here, first-forbidden transitions related to the decay of a $0g_{9/2}$ neutron into a $0h_{9/2}$ proton are also expected.

The $pn$-QRPA predictions show an odd-even $Z$ staggering around the experimental values that fades away after crossing the 126-neutron shell closure. For the moderate-$Q_\beta$ nuclei discussed, this effect might be due to the discrepancies between calculated and experimental single-particle energies that enhance the sensitivity of the calculations to transitions decaying to a limited number of low-lying states [11]. Even so, the deviations, less pronounced than for the FRDM + QRPA calculations, are predicted to vanish for the $Z = 64$–74 nuclei, providing values very close to those of SM [11]. For DF3 + cQRPA, calculated half-lives generally match the measured values within a factor of 2, with the exception of $^{199}$Ir and $^{212}$Tl. In these latter cases, the over- or underestimation of the experimental results seems spurious, probably due to the fact that the effective $NN$ interaction used is the same for all mass numbers. For the SM, computational requirements limit the current half-life estimates to nuclei very close to

the $N = 126$ shell [9]. Predicted values for $^{203,204}$Pt are in excellent agreement with the experimental half-lives, indicating that fully self-consistent microscopic models [7,9] better reproduce the lifetimes in the $N \sim 126$ region spanned by the $r$-process during the freeze-out stage.

In conclusion, the half-lives discussed provide a significant constraint on the theories used to calculate $\beta$-decay properties for nucleosynthesis modeling. The results show a reduction of the standard $r$-process lifetimes of more than 1 order-of-magnitude in the $Z < 82$, $N < 126$ quadrant and are in better agreement with the predictions of full microscopic treatments for the total $\beta$ strength. This suggests a substantial contribution from high-energy, first-forbidden transitions in this mass region. Further measurements at the new generation of nuclear facilities will test the persistence of the observed tendencies in lighter $N = 126$ nuclei. At present, these results are the closest experimental information on $\beta$ decay relative to the $A \sim 195$ $r$-abundance peak progenitors and pave the way for a better understanding of the $r$-process matter flow to heavier fissioning nuclei.

The excellent work of the GSI accelerator staff is acknowledged. This work was supported by the Spanish MICINN under Grants No. FPA2007-62652, No. FPA2008-6419-C02-01, and No. FPU-AP2007-04543 and by the program Ingenio 2010, Consolider CPAN, the Galician Regional Government under Unidades Competitivas 2010/57, the BMBF under Grant No. 06KY9136I, the National Measurement Office (NMO), EPSRC, and STFC (UK), the EU Access to Large Scale Facilities Programme (Eurons, EU Contract No. 506065), The Swedish Research Council, the German BMBF, and the Italian INFN. We thank I. N. Borzov, T. Suzuki, and Dong-Liang Fang for valuable discussions.

*anaisabel.morales@mi.infn.it
Present address: INFN, Università degli Studi di Milano, I-20133 Milano, Italy.
†Present address: Centre d'Etudes Nucléaires de Bordeaux Gradignan IN2P3/CNRS-Université Bordeaux, F-33170, Gradignan, France.
‡Present address: Department of Physics and Astrophysics, University of Delhi, Delhi 110007, India.
§Present address: GSI, Planckstrasse 1, D-64291 Darmstadt, Germany.
¶Present address: Universidade de Vigo, 36310 Vigo, Spain.
**Present address: KACST, P.O. Box 6086, Riyadh 11442, Saudi Arabia.
††Present address: Comisión Chilena de Energía Nuclear, P.O. Box 188-D, Santiago de Chile, Chile.
‡‡Present address: Physik-Department E12, TU München, D-85748 Garching, Germany.

[1] E. M. Burbidge, G. R. Burbidge, W. A. Fowler, and F. Hoyle, Rev. Mod. Phys. **29**, 547 (1957).
[2] N. R. C. Committee on the Physics of the Universe, *Connecting Quarks with the Cosmos: Eleven Science Questions for the New Century* (The National Academies Press, Washington, DC, 2003).
[3] C. Sneden, J. Cowan, and R. Gallino, Annu. Rev. Astron. Astrophys. **46**, 241 (2008).
[4] K.-L. Kratz, F.-K. Thielemann, W. Willebrandt, P. Moller, V. Harms, A. Wohr, and J. W. Truran, J. Phys. G **14**, S331 (1988).
[5] R. Surman, M. Mumpower, J. Cass, I. Bentley, A. Aprahamian, and G. C. McLaughlin, Eur. Phys. J. Web Conf. **66**, 07024 (2014).
[6] P. Möller, B. Pfeiffer, and K.-L. Kratz, Phys. Rev. C **67**, 055802 (2003).
[7] I. N. Borzov, Phys. Rev. C **67**, 025802 (2003).
[8] I. N. Borzov, Phys. At. Nucl. **74**, 1435 (2011).
[9] T. Suzuki, T. Yoshida, T. Kajino, and T. Otsuka, Phys. Rev. C **85**, 015802 (2012).
[10] Q. Zhi, E. Caurier, J. Cuenca-García, K. Langanke, G. Martínez-Pinedo, and K. Sieja, Phys. Rev. C **87**, 025803 (2013).
[11] D.-L. Fang, B. A. Brown, and T. Suzuki, Phys. Rev. C **88**, 034304 (2013).
[12] B. Pfeiffer, K.-L. Kratz, F.-K. Thielemann, and W. B. Walters, Nucl. Phys. **A693**, 282 (2001).
[13] I. Dillmann *et al.*, Phys. Rev. Lett. **91**, 162503 (2003).
[14] B. Ekström, B. Fogelberg, P. Hoff, E. Lund, and A. Sangariyavanish, Phys. Scr. **34**, 614 (1986).
[15] R. Gill, R. Casten, D. Warner, A. Piotrowski, H. Mach, J. Hill, F. Wohn, J. Winger, and R. Moreh, Phys. Rev. Lett. **56**, 1874 (1986).
[16] K.-L. Kratz, H. Gabelmann, W. Hillebrandt, B. Pfeiffer, K. Schlösser, and F.-K. Thielemann, Z. Phys. A **325**, 489 (1986).
[17] A. Jungclaus *et al.*, Phys. Rev. Lett. **99**, 132501 (2007).
[18] S. Nishimura *et al.*, Phys. Rev. Lett. **106**, 052502 (2011).
[19] O. Arndt *et al.*, Phys. Rev. C **84**, 061307 (2011).
[20] M. Madurga *et al.*, Phys. Rev. Lett. **109**, 112501 (2012).
[21] E. Caurier, G. Martinez-Pinedo, F. Nowacki, A. Poves, and A. P. Zuker, Rev. Mod. Phys. **77**, 427 (2005).
[22] H. Álvarez-Pol *et al.*, Phys. Rev. C **82**, 041602 (2010).
[23] T. Kurtukián-Nieto *et al.*, Phys. Rev. C **89**, 024616 (2014).
[24] T. Kurtukián-Nieto, J. Benlliure, and K.-H. Schmidt, Nucl. Instrum. Methods Phys. Res., Sect. A **589**, 472 (2008).
[25] T. Kurtukián-Nieto *et al.*, Nucl. Phys. **A827**, 587 (2009).
[26] Z. Podolyák *et al.*, Phys. Lett. B **672**, 116 (2009).
[27] G. Benzoni *et al.*, Phys. Lett. B **715**, 293 (2012).
[28] N. Al-Dahan *et al.*, Phys. Rev. C **85**, 034301 (2012).
[29] A. I. Morales *et al.*, Phys. Rev. C **89**, 014324 (2014).
[30] G. Benzoni and A. I. Morales, Eur. Phys. J. Web Conf. **66**, 02007 (2014).
[31] H. Geissel *et al.*, Nucl. Instrum. Methods Phys. Res., Sect. B **70**, 286 (1992).
[32] R. Kumar *et al.*, Nucl. Instrum. Methods Phys. Res., Sect. A **598**, 754 (2009).
[33] S. Pietri *et al.*, Nucl. Instrum. Methods Phys. Res., Sect. B **261**, 1079 (2007).
[34] A. I. Morales *et al.*, Phys. Rev. C **84**, 011601 (2011).
[35] A. I. Morales *et al.*, Phys. Rev. C **88**, 014319 (2013).
[36] D. Craig and H. Taylor, J. Phys. G **10**, 1133 (1984).
[37] T. Suzuki (private communication).
[38] C. Wennemann, W.-D. Schmidt-Ott, T. Hild, K. Krumbholz, V. Kunze, F. Meissner, H. Keller, R. Kirchner, and E. Roeckl, Z. Phys. A **347**, 185 (1994).